

Interferometric Tests of Teleportation

T.C.Ralph

*Department of Physics, Centre for Lasers,
The University of Queensland,
St Lucia 4072 Australia
E-mail: ralph@physics.uq.edu.au*

(December 2000)

Abstract

We investigate a direct test of teleportation efficacy based on a Mach-Zehnder interferometer. The analysis is performed for continuous variable teleportation of both discrete and continuous observables.

I. INTRODUCTION

Information is not independent of the physical laws used to store and process it [1]. The unique properties of quantum mechanics lead to radically different ways of communicating and processing information [2]. The study of quantum information is currently one of the fastest growing areas of physics.

Quantum teleportation [3–7] is a method by which quantum information can be passed through a classical channel and successfully retrieved at a distant location. The sharing of entanglement between the sender (Alice) and receiver (Bob) is essential for teleportation as it provides the “quantum key” needed to retrieve the quantum information [8]. In this way an unknown quantum state of an object can be transferred through a classical channel, with neither Bob nor Alice knowing the state.

The efficacy of teleportation can be characterized in two quite distinct ways. Traditionally fidelity is used for this purpose [9]. Fidelity, F , gives a measure of the quality of the teleported state by evaluating the overlap between the input state, $|\psi\rangle$, and the teleported output state, ρ , via $F = \langle\psi|\rho|\psi\rangle$. Fidelity is state dependent, ie the fidelity of the reconstructed state depends both on the quality of the teleporter and on the class of input states from which the unknown state is picked. More recently the amplitude conditional variance between the input and output has been suggested as an alternative measure [10,11]. The conditional variance measures the amount of uncorrelated noise that is added to the quantum state in the teleportation process. As such it is a measure of the quality of the teleporter itself, independent of the state to be teleported. The measurement of either fidelity or the conditional variance involves a “third” person, Victor (the verifier), who prepares the input

states and examines the teleported states to determine the quality of the teleportation. For example Victor may prepare photons in particular polarisation states and then check if they are still in the same states after teleportation [4,5]. For continuous variable experiments the signal and noise properties of the input and output are compared [7,12].

Another way of testing the efficacy of teleportation is to create a pair of quantum correlated objects, teleport one of them, then test directly to what extent they are still quantum correlated. An example of this is polarization entanglement swapping [6] in which one of an entangled pair of photons is teleported and then the degree of entanglement that remains between them is measured. A version of this experiment using continuous variable teleportation has also been proposed [14]. Another possibility is to teleport one arm of a spatial superposition and then measure the preservation of the superposition directly through their interference characteristics. These types of tests are important for 3 reasons: (i) They directly observe the preservation of quantum correlations rather than just inferring them; (ii) such specific situations highlight aspects of the physics of the teleportation process not obvious from considering more general figures of merit and; (iii) from a practical point of view the preservation of entanglement and interference effects will be an important aspect of teleportation in most quantum processing applications.

A spatial superposition test can be applied to single photon polarization states using a Mach-Zehnder interferometer [13]. An interesting feature of such a test is that it is possible for Alice and Bob to verify that their teleporter is operating correctly without knowing the input states. In this paper we generalize this test to cover a broad range of input states, including continuous variable states. We will begin, in section 2, by introducing the model for a teleporter we will use throughout the paper. In section 3 we will review the operation of the Mach-Zehnder interferometer as a teleportation tester for single photon, polarisation superposition inputs. Section 4 will examine more general low photon number states. In section 5 we will generalize the technique to input states with continuous degrees of freedom and in section 6 we will discuss and conclude.

II. THE TELEPORTER

The teleporter we will consider in this paper is an all optical device using continuous variable (squeezing) entanglement as a quantum resource [15]. This model is chosen for its versatility in being able to teleport all the input states considered in this paper. In an experimental situation more input specialized devices may be used. Consider first the “classical teleportation” device depicted in Fig.1(a). By classical we mean we attempt to transfer the quantum information through a classical channel without the assistance of entanglement. The input light field, $\hat{a}_{in}(t)$, is sent through a linear optical amplifier by Alice. In Fourier space the output of a linear amplifier can be written

$$a_c(\omega) = \sqrt{\eta_a G(\omega)} a_{in}(\omega) + \sqrt{(G(\omega) - 1)} v_1^\dagger + \sqrt{G(\omega)(1 - \eta_a)} v_a \quad (1)$$

where $G(\omega)$ is the (frequency dependent) amplifier gain and v_1 and v_a are vacuum noise inputs due to the gain and internal losses (η_a) of the amplifier respectively. If the gain is sufficiently large ($G \gg 1$) then a_c can be regarded as a classical field. This is because the conjugate quadrature variables $X_c^+ = a_c + a_c^\dagger$ and $X_c^- = i(a_c - a_c^\dagger)$ both have uncertainties

much greater than the quantum limit, i.e. $\Delta(X_c^\pm)^2 \gg 1$. This means that simultaneous measurements of the conjugate quadratures can extract all the information carried by a_c with negligible penalty. The quantum noise added due to the simultaneous measurements will be negligible compared to the amplified quadrature uncertainties. It is thus possible to convert then transmit the information carried in this beam over any available classical channel (radio, copper wires, etc). However it is convenient, and no less general, to retain an optical classical channel. Further discussion and a simple proof of the classical nature of this channel can be found in the appendix.

When Bob receives the classical beam he attempts to retrieve the quantum state of the input by simply attenuating the beam with a beamsplitter of transmission ε . The output field is $a_{out} = \sqrt{\varepsilon}a_c - \sqrt{1-\varepsilon}v_2$ where v_2 is the vacuum mode incident on the unused port of the beamsplitter. The final output field is thus

$$a_{out}(\omega) = \lambda(\omega)a_{in}(\omega) + \left(\frac{\lambda(\omega)}{\sqrt{\eta_a}}v_1^\dagger - v_2\right) + \lambda(\omega)\frac{\sqrt{1-\eta_a}}{\sqrt{\eta_a}}v_a \quad (2)$$

where the total classical channel gain is given by $\lambda(\omega) = \sqrt{G(\omega)\varepsilon\eta_a}$ and we have assumed the classical channel limit $G \rightarrow \infty$ and $\varepsilon \rightarrow 0$. In practice we are only interested in finite bandwidths. For photon counting experiments this usually means frequency filters will be placed in front of the detectors. For continuous variable experiments only a finite range of RF frequencies will be analyzed. We will assume that the optical amplifier, and thus λ has a flat response over the detection bandwidth. Hence, setting unity gain ($\lambda = 1$) and negligible loss ($\eta_a = 1$) we obtain the usual result

$$a_{out} = a_{in} + v_1^\dagger - v_2 \quad (3)$$

whereby two vacuum noise penalties are imposed by classical teleportation [16,10].

Quantum teleportation can be achieved by replacing the independent vacuum inputs, v_1 and v_2 , with Einstein, Podolsky, Rosen (EPR) entangled beams [17], b_1 and b_2 , as shown in Fig.1(b). Such beams have the very strong correlation property that both their difference amplitude quadrature variance, $\Delta(X_{b1}^+ - X_{b2}^+)^2$, and their sum phase quadrature variance, $\Delta(X_{b1}^- + X_{b2}^-)^2$, are less than the quantum limit ($=1$). Such beams can be generated by sub-threshold non-degenerate parametric amplification [17] or by the mixing of independent squeezed sources [18,10]. For non-degenerate parametric amplification these beams can be represented by

$$\begin{aligned} b_1(\omega) &= \sqrt{\eta_{b1}H(\omega)}v_3 + \sqrt{\eta_{b1}(H(\omega) - 1)}v_4^\dagger + \sqrt{1 - \eta_{b1}}v_{b1} \\ b_2(\omega) &= \sqrt{\eta_{b2}H(\omega)}v_4 + \sqrt{\eta_{b2}(H(\omega) - 1)}v_3^\dagger + \sqrt{1 - \eta_{b2}}v_{b2} \end{aligned} \quad (4)$$

where $H(\omega)$ is the parametric gain and as before the η 's and v 's are efficiencies and resultant vacuum inputs respectively. The strength of the squeezing entanglement can be characterized by $V_{ent} = (\sqrt{H} - \sqrt{H-1})^2$ which varies from not entangled ($V_{ent} = 1$) to strongly entangled ($V_{ent} \rightarrow 0$) as the parametric gain increases. We will also refer to the percentage of entanglement squeezing as $(1 - V_{ent}) \times 100\%$. The output field is now given by

$$a_{out}(\omega) = \lambda(\omega)a_{in}(\omega) + \left(\frac{\lambda(\omega)}{\sqrt{\eta}}b_1^\dagger(\omega) - b_2(\omega)\right) + \lambda(\omega)\frac{\sqrt{1-\eta}}{\sqrt{\eta}}v_a \quad (5)$$

which, because of the strong correlations between b_1 and b_2 , reduces to

$$a_{out}(\omega) = \lambda(\omega)a_{in}(\omega) + (\lambda(\omega)\sqrt{H(\omega)} - \sqrt{H(\omega) - 1})v_3^\dagger + (\sqrt{H(\omega)} - \lambda\sqrt{H(\omega) - 1})v_4 \quad (6)$$

in the absence of losses ($\eta_a = \eta_{b1} = \eta_{b2} = 1$). Again we assume (and will do so for the remainder of the paper) that all gains are flat across the detection bandwidth. In the limit of very high parametric gain ($H \rightarrow \infty$, $V_{ent} \rightarrow 0$) and unity classical channel gain ($\lambda = 1$) the output becomes identical to the input ($a_{out} \rightarrow a_{in}$). This is ideal quantum teleportation as the only direct link between the input and output is the classical field a_c , yet arbitrarily accurate reconstruction of the input state is, in principle, possible with a sufficiently strong EPR correlation. The uncertainty principle is not compromised because the variances of each of the quadratures of b_1 by themselves are very noisy. Thus the information about a_{in} carried on the classical field is buried in this noise and cannot be extracted by using the classical field alone. An important operating point is the classical channel gain $\lambda_{opt} = \frac{\sqrt{H-1}}{\sqrt{H}}$. With this gain, in the absence of losses, the output field is given by

$$a_{out} = \lambda_{opt}a_{in} + (\sqrt{1 - \lambda_{opt}^2})v_4 \quad (7)$$

i.e. it is simply an attenuated version of the input [14]. The teleporter can be generalized to deal with arbitrary polarisations of the input field by decomposing the field into orthogonal polarisation components (using a polarising beamsplitter) and teleporting the individual components separately (see Fig.1(c)).

The question remains as to how the linear amplifier in Fig.1 could be constructed. This is not trivial as in standard optical amplifiers the source of the vacuum mode is not available for modification. For example, in a laser amplifier the physical origin of the vacuum input (v_1) is collisionally or phonon induced dipole fluctuations of the gain medium [19]. One solution is shown schematically in Fig.2. The input beam is mixed with the EPR beam, b_1 , at a 50:50 beamsplitter. The output beams are

$$\begin{aligned} c &= \frac{1}{\sqrt{2}}(a_{in} + b_1) \\ d &= \frac{1}{\sqrt{2}}(a_{in} - b_1) \end{aligned} \quad (8)$$

The beams are amplified by degenerate parametric amplifiers of equal gains but with a π phase shift between there pump (E) phases. This results in the outputs

$$\begin{aligned} c' &= \sqrt{G}c + \sqrt{G-1}c^\dagger \\ d' &= \sqrt{G}d - \sqrt{G-1}d^\dagger \end{aligned} \quad (9)$$

Recombining these beams on a beamsplitter then produces the desired output: $a_c = \sqrt{G}a_{in} + \sqrt{G-1}b_1^\dagger$.

III. THE MACH-ZEHNDER INTERFEROMETER AND THE TELEPORTER

We now examine the efficacy of the teleporter described in the previous section as characterized using an interferometer. In this section we will consider idealized single photon

polarisation superpositions as inputs to illustrate the basic physics. In the next section we will consider more general polarisation-number inputs. In the following section continuous variable inputs will be considered.

Consider first the set-up shown schematically in Fig.3(a) (see also Fig.4(a)). Basically we place a teleporter in one arm of a Mach-Zehnder interferometer, inject a single photon state, in an arbitrary polarisation superposition state into one port, then use the interference visibility at the output ports to characterize the efficacy of teleportation. A useful feature of this set-up is the visibility does not depend on the input state of the single photon, so we can assess how well the teleporter is working without knowing what is going into it. Let us see how this works.

The input for one port of the interferometer is in the arbitrary polarisation superposition state

$$|\phi\rangle_a = x|1, 0\rangle + y|0, 1\rangle \quad (10)$$

where $|n_h, n_v\rangle \equiv |n_h\rangle_h \otimes |n_v\rangle_v$, n_h and n_v are the photon number in the horizontal and vertical polarisations respectively, and $|x|^2 + |y|^2 = 1$. The input of the other port is in the vacuum state $|\phi\rangle_b = |0, 0\rangle$. The operators in the Heisenberg picture for the four input modes (two spatial times two polarisation) are a_h and a_v (superposition), and b_h and b_v (vacuum). We propagate these operators through the Mach-Zehnder (including the teleporter). After the first beamsplitter we can write

$$\begin{aligned} c_{h,v} &= \frac{1}{\sqrt{2}}(a_{h,v} + b_{h,v}) \\ d_{h,v} &= \frac{1}{\sqrt{2}}(a_{h,v} - b_{h,v}) \end{aligned} \quad (11)$$

One of the beams (c) is then teleported. Under conditions for which losses can be neglected we can use Eq. 6 to obtain

$$c_{h,v,T} = \lambda c_{h,v} + (\lambda\sqrt{H} - \sqrt{H-1})b_{h,v,1}^\dagger + (\sqrt{H} - \lambda\sqrt{H-1})b_{h,v,2} \quad (12)$$

The fields are recombined in phase at the final beamsplitter giving the outputs

$$\begin{aligned} a_{h,v,out} &= \frac{1}{\sqrt{2}}(c_{h,v,T} + d_{h,v}) \\ b_{h,v,out} &= \frac{1}{\sqrt{2}}(c_{h,v,T} - d_{h,v}) \end{aligned} \quad (13)$$

The expectation values for photon counting at the two outputs of the interferometer are

$$\begin{aligned} \langle a_{out}^\dagger a_{out} \rangle &= \langle \phi|_a \langle \phi|_b \langle \phi|_f (a_{h,out}^\dagger + a_{v,out}^\dagger)(a_{h,out} + a_{v,out}) |\phi\rangle_a |\phi\rangle_b |\phi\rangle_f \\ &= 0.25(1 + \lambda)^2 + (\lambda\sqrt{H} - \sqrt{H-1})^2 \\ \langle b_{out}^\dagger b_{out} \rangle &= \langle \phi|_a \langle \phi|_b \langle \phi|_f (b_{h,out}^\dagger + b_{v,out}^\dagger)(b_{h,out} + b_{v,out}) |\phi\rangle_a |\phi\rangle_b |\phi\rangle_f \\ &= 0.25(1 - \lambda)^2 + (\lambda\sqrt{H} - \sqrt{H-1})^2 \end{aligned} \quad (14)$$

In the limit of very strong entanglement squeezing ($V_{ent} \rightarrow 0$) we find from Eq. 12 that $c_{h,v,T} \rightarrow c_{h,v}$ for unity gain ($\lambda = 1$), i.e. perfect teleportation. For the same conditions (and only for these conditions) the visibility of the Mach-Zehnder outputs,

$$\mathcal{V} = \frac{\langle a_{out}^\dagger a_{out} \rangle - \langle b_{out}^\dagger b_{out} \rangle}{\langle a_{out}^\dagger a_{out} \rangle + \langle b_{out}^\dagger b_{out} \rangle} \quad (15)$$

goes to one, indicating the state of the teleported arm exactly matches that of the unteleported arm. Notice that the expectation values (Eq.14), and thus the visibility, do not depend on the actual input state (no dependence on x and y). Hence we can demonstrate that the teleporter is operating ideally even if we do not know the state of the input. Classical limits can be set by examining the visibility obtained with no entanglement ($H = 1$). In Fig.5 we plot the visibility versus feedforward gain in the teleporter for the cases of no entanglement (0%), 50% entanglement squeezing and 90% entanglement squeezing. Maximum visibility occurs for the gain condition

$$\lambda = \frac{\sqrt{4H - 3}}{\sqrt{4H + 1}} \quad (16)$$

giving $\mathcal{V}_{max,c} = \sqrt{1/5}$ as the maximum visibility that can be obtained in the absence of entanglement. Increasing entanglement leads to increasing maximum visibility.

In the experiments we have imagined so far the level of visibility has been determined not only by the ability of the teleporter to reproduce the input polarisation states of the photons (the mode overlap) but also the efficiency with which input photons to the teleporter lead to correct output photons (the power balance). It is of interest to try to separate these effects. We can investigate just state reproduction if we allow attenuation to be applied to beam d , thus “balancing” the Mach-Zehnder Interferometer by compensating for the loss introduced by the teleporter (see Fig.3(b)). The attenuated beam d becomes

$$d_{h,v,A} = \sqrt{\eta}d_{h,v} + \sqrt{1 - \eta}g_{h,v} \quad (17)$$

where g is another vacuum field and η is the intensity transmission of the attenuator. The expectation values of the outputs are now

$$\begin{aligned} \langle a_{out}^\dagger a_{out} \rangle &= 0.25(\sqrt{\eta} + \lambda)^2 + (\lambda\sqrt{H} - \sqrt{H - 1})^2 \\ \langle b_{out}^\dagger b_{out} \rangle &= 0.25(\sqrt{\eta} - \lambda)^2 + (\lambda\sqrt{H} - \sqrt{H - 1})^2 \end{aligned} \quad (18)$$

In Fig.6 we plot visibility versus gain, using the attenuation η to optimize the visibility ($\eta \leq 1$). Now we can always achieve unit visibility for any finite level of entanglement by operating at gain

$$\lambda_{opt} = \frac{\sqrt{H - 1}}{\sqrt{H}} \quad (19)$$

and balancing the interferometer by setting $\eta = \lambda_{opt}^2$. The high visibility is achieved because at gain λ_{opt} the teleporter behaves like pure attenuation (see Eq. 7). That is the photon flux of the teleported field is reduced, but no “spurious photons” are added to the field. Thus, at this gain, all output photons from the teleporter are in the right state, but various input photons are “lost”.

This contrast between state-reproduction and efficiency has been a topic of vigorous debate [21,22]. It is of note that our interferometric test can separate the two effects. It

should also be noted that our test is sensitive not only to the relative phase of the polarisation superposition, but also the overall phase of the teleported field. The overall phase is defined with respect to the field in the unteleported arm of the interferometer and is a constituent of the mode-overlap. If the overall phase is randomized by the teleporter then very low visibility will result from our interferometric test. At the end of section IV we will examine an interesting consequence of this additional sensitivity.

We now consider the effect of propagation loss in the two arms of the entangled source. Hence, referring back to Eq.5, we set $\eta_{b1} = \eta_{b2} = \eta_b \neq 1$. We neglect for the moment the possibility of internal loss in the amplification (i.e. $\eta_a = 1$) or unequal loss in the two arms. With loss present (but not balancing the interferometer) the maximum visibility is achieved with the gain condition

$$\lambda_{max} = \frac{\sqrt{4(H-1)+1}}{\sqrt{4(1-\eta_b)+4\eta_b H+1}} \quad (20)$$

In Fig.7(a) we plot maximum visibility as a function of loss for various levels of entanglement squeezing. Visibility is reduced quite rapidly. If balancing of the interferometer is allowed the gain condition for maximum visibility remains that found for no loss (Eq.19) but the balancing condition becomes $\eta = (5 - 4\eta_b)\lambda^2$. Once again visibility drops off rapidly with increasing loss (see Fig.7(b)) tending eventually to the classical limit as the loss completely wipes out the entanglement.

The effect of loss in the amplification (or measurement stage) ($\eta_a \neq 1$) produces very similar results to those in Fig.7, as does indeed loss in only the entanglement arm sent to Alice (b_1). However if loss is only present in the entanglement arm sent to Bob ($\eta_{b1} = 1, \eta_{b2} \neq 1$) things are rather different. The unbalanced visibility is still reduced with increasing loss but when the interferometer is balanced one can still achieve unit visibility by operating at the gain condition

$$\lambda_{opt} = \frac{\sqrt{\eta_{b2}(H-1)}}{\sqrt{H}} \quad (21)$$

Although the visibility is maintained the efficiency is of course dropping. In the limit of strong loss, $\eta_{b2} \rightarrow 0$, the efficiency goes to zero and no photons are teleported.

IV. MORE GENERAL POLARISATION INPUT STATES

So far we have assumed that the input state is a single photon number state. That is there is unit probability that one, and only one, photon arrives per measurement interval. Such states are yet to be demonstrated experimentally, though candidate sources have been proposed [23,24]. However the results of the previous section don't actually rely on the input being in a number state. An examination of Eq.14 shows that it is only the *expectation value* of the photon number which is important. Thus any input state with an average photon number of one count per measurement interval will give identical visibilities as those of the previous section. An example is the low photon number coherent state $|\phi\rangle = |\alpha_h, \alpha_v\rangle$, in which $|\alpha_h|^2 + |\alpha_v|^2 = 1$. Such a state can approximately be produced by strongly attenuating

a stable laser beam. We can generalize Eq.14 for arbitrary average input photon number (\bar{n}) to obtain

$$\begin{aligned}\langle a_{out}^\dagger a_{out} \rangle &= \bar{n}0.25(1+\lambda)^2 + (\lambda\sqrt{H} - \sqrt{H-1})^2 \\ \langle b_{out}^\dagger b_{out} \rangle &= \bar{n}0.25(1-\lambda)^2 + (\lambda\sqrt{H} - \sqrt{H-1})^2\end{aligned}\quad (22)$$

Maximum visibility now occurs for the gain condition

$$\lambda_{max} = \frac{\sqrt{4H + \bar{n} - 4}}{\sqrt{4H + \bar{n}}}\quad (23)$$

giving $\mathcal{V}_{max,c} = \sqrt{\bar{n}/(\bar{n} + 4)}$ for the maximum classical visibility. As might be expected higher maximum visibilities can be achieved with only a classical channel as the average photon number increases and the input becomes more like a classical field. For average photon numbers less than one the maximum achievable visibility is reduced. This is basically a signal to noise effect. The penalty in classical teleportation arises from amplification of vacuum fluctuations (v_1) introduced in the “measurement” process. For low photon numbers this noise is large compared to the signal leading to low visibility. For large photon numbers the noise can become negligible compared to the signal leading to high visibilities. Fig.8 illustrates the change in λ_{max} and V_{max} as a function of entanglement for various values of the input photon number.

Single photon number states can be realized conditionally by using number entangled states. It is instructive to investigate this special case (see Fig.4(b)). A low efficiency, non-degenerate parametric amplifier (down converter) can produce pairs of photons in the polarisation-number entangled state

$$|\phi\rangle_{a,a'} \approx |0,0\rangle_a |0,0\rangle_{a'} + \chi(|1,0\rangle_a |1,0\rangle_{a'} + |0,1\rangle_a |0,1\rangle_{a'})\quad (24)$$

where a and a' are the two, spatially separated fields and χ is the conversion efficiency. We have assumed $\chi \ll 1$ and neglected higher order terms in χ . As before a is the input field to the interferometer plus teleporter and is transformed as per Eq.13. We can either analyze the raw visibility of the outputs or the conditional visibility. Beam a by itself is in the unpolarised mixed state, given by the reduced density operator

$$\rho_a \approx |0,0\rangle\langle 0,0| + \chi^2(|0,1\rangle\langle 0,1| + |1,0\rangle\langle 1,0|)\quad (25)$$

The raw count rates are thus calculated using $\langle a^\dagger a \rangle = Tr[\rho a^\dagger a]$. As would be expected the raw visibility is as predicted by Eq.22 with $\bar{n} = \chi^2$. Because χ is small, classical teleportation visibilities will be low. However with teleportation entanglement they can, in principle, reach unity. It is important to note that the commonly used measure of teleportation, fidelity, cannot be used to judge teleportation of such a mixed state [25]. The fidelity between mixed input and output states is defined by [26]

$$F = Tr[\sqrt{\rho_a^{1/2} \rho_{out} \rho_a^{1/2}}]\quad (26)$$

If $\rho_a = \rho_{out}$ then $F = 1$. But this can easily be arranged by a cheating Alice and Bob without using entanglement. This is because *any* unpolarised mixed state with average photon

number χ^2 will have a density operator equal to ρ_a . Only by making measurements of the joint state of a and a' before and after the teleporter and calculating a global fidelity can a high fidelity be considered proof of quantum teleportation. In contrast a local interferometric test on only a unambiguously judges the quality of the teleporter. This is due to the sensitivity of the teleporter to the overall phase of the field. As a result high visibilities are only possible when Alice and Bob share entanglement.

Conditional visibilities can be obtained by making the coincidence counts $\langle\phi|_{a,a'}\langle\phi|_b a'^{\dagger} a' a_{out}^{\dagger} a_{out} |\phi\rangle_b |\phi\rangle_{a,a'}$ and $\langle\phi|_{a,a'}\langle\phi|_b a'^{\dagger} a' b_{out}^{\dagger} b_{out} |\phi\rangle_b |\phi\rangle_{a,a'}$. Now counts are only recorded if a photon has simultaneously been detected in beam a' . This guarantees that only counts corresponding to times when a photon is launched into the interferometer are recorded. The visibilities then correspond to those obtained in section 2 with single photon input states. This result is conceptually different from the case of an average of one photon per measurement interval because it can be arranged, to a high probability, that only one photon is ever present at one time in the interferometer.

V. CONTINUOUS VARIABLE INPUTS

We now consider a very different type of input state and detection technique. Our input beam will now potentially be a “bright” beam. However our interest will centre only on the state of the “side-bands” of the beam at some RF frequencies $\pm\omega$ around the central frequency. We will require that ω is sufficiently large that the power in the side-bands at that frequency are of the order of one photon per second. Typically, for solid-state lasers, $\omega \gg 10\text{MHz}$ will suffice. Instead of considering the polarisation state of the light, as in the previous sections, we will now consider the field state of the side-bands, as characterized by their distribution of power between phase and amplitude fluctuations. The total power in the side-bands at the outputs can be measured using optical homodyne techniques and visibilities constructed. These visibilities behave identically to those in the photon counting case provided the average photon number in the sidebands is equal to \bar{n} . This is quite surprising given the incompleteness of the formal analogy between single photon polarisation states and single mode continuous variable states.

The proposed set-up is shown in Fig.4(c). It is identical to that for the single photon input except for the homodyne detection systems at the outputs instead of photon counters. The output beams are divided in half at beamsplitters and sent to homodyne detectors which detect orthogonal quadrature amplitudes, i.e.

$$\begin{aligned} X^+(\omega) &= e^{i\theta} a(\omega) + e^{-i\theta} a^{\dagger}(\omega) \\ X^-(\omega) &= e^{i(\theta+\pi/2)} a(\omega) + e^{-i(\theta+\pi/2)} a^{\dagger}(\omega) \end{aligned} \quad (27)$$

where the absolute quadrature angle, θ , is arbitrary. Although the homodyne detection itself can be ideal, the splitting of the beams at the beamsplitters inevitably introduces vacuum noise (this must occur because orthogonal quadratures constitute conjugate observables). Thus the detection results are

$$X_a^+(\omega) = \frac{1}{\sqrt{2}}(a_{out}(\omega) + a_{out}^{\dagger}(\omega) + v_{d1} + v_{d1}^{\dagger})$$

$$\begin{aligned}
X_a^-(\omega) &= \frac{i}{\sqrt{2}}(a_{out}^\dagger(\omega) - a_{out}(\omega) + v_{d1} - v_{d1}^\dagger) \\
X_b^+(\omega) &= \frac{1}{\sqrt{2}}(b_{out}(\omega) + b_{out}^\dagger(\omega) + v_{d2} + v_{d2}^\dagger) \\
X_b^-(\omega) &= \frac{i}{\sqrt{2}}(b_{out}^\dagger(\omega) - b_{out}(\omega) + v_{d2} - v_{d2}^\dagger)
\end{aligned} \tag{28}$$

where the arbitrary angle, θ has been set to zero for simplicity. The penalty vacuum noise is represented as usual by v 's. Consider adding the photocurrents from each beam with a $\pi/2$ phase shift. This could be achieved by imposing a delay of τ to one of the currents such that $\tau\omega = \pi/2$. This gives photocurrents

$$\begin{aligned}
A(\omega) &= X_a^+ + iX_a^- = \sqrt{2}(a_{out} + v_{d1}^\dagger) \\
B(\omega) &= X_b^+ + iX_b^- = \sqrt{2}(b_{out} + v_{d2}^\dagger)
\end{aligned} \tag{29}$$

These photocurrents could then be fed into spectrum analyzers which give the photon number spectra

$$\begin{aligned}
V_A(\omega) &= \langle |X_a^+ + iX_a^-|^2 \rangle = 2\langle a_{out}^\dagger(\omega)a_{out}(\omega) \rangle + 2 \\
V_B(\omega) &= \langle |X_b^+ + iX_b^-|^2 \rangle = 2\langle b_{out}^\dagger(\omega)b_{out}(\omega) \rangle + 2
\end{aligned} \tag{30}$$

We can then define, in analogy with the photon counting case (Eq.15), the spectral visibility as

$$\begin{aligned}
\mathcal{V} &= \frac{\langle a_{out}^\dagger(\omega)a_{out}(\omega) \rangle - \langle b_{out}^\dagger(\omega)b_{out}(\omega) \rangle}{\langle a_{out}^\dagger(\omega)a_{out}(\omega) \rangle + \langle b_{out}^\dagger(\omega)b_{out}(\omega) \rangle} \\
&= \frac{V_A - V_B}{V_A + V_B - 4}
\end{aligned} \tag{31}$$

Note that for an arbitrary field we can also write

$$V_{In}(\omega) = \langle |X^+ + iX^-|^2 \rangle = V^+ + V^- - 2 \tag{32}$$

where $V^+ = \langle |X^+|^2 \rangle$ and $V^- = \langle |X^-|^2 \rangle$. Hence we can make the identification

$$\langle a_{in}^\dagger(\omega)a_{in}(\omega) \rangle = \frac{1}{4}(V^+ + V^-) - \frac{1}{2} \tag{33}$$

Eq.33 allows us to construct visibilities directly from individually measured orthogonal quadrature spectral variances. Also it allows us to compare the visibilities obtained here with those of the previous sections. In order to make such comparisons with the photon counting visibilities we observe that $\langle a_{in}^\dagger(\omega)a_{in}(\omega) \rangle$ is the photon number in the upper frequency component of the field only. Thus the total average photon number of upper and lower side-bands (assuming a frequency symmetric input state) is $\bar{n}(\pm\omega) = 2\langle a_{in}^\dagger(\omega)a_{in}(\omega) \rangle$. This is similar to the summing of the average photon numbers for both polarization modes in the discrete case. For equivalent average photon numbers (Eq.22 with $\bar{n}(\pm\omega) \equiv \bar{n}$) *all* the predictions of the low photon number visibilities are exactly reproduced in the continuous variable case, including the ability to re-balance the interferometer and obtain unit visibilities.

The preceding analysis has shown that interferometric tests of quantum teleportation for unknown continuous variable states of a fixed average photon number can also be performed. Let us consider a couple of examples. For an arbitrary input field there will be some particular value of θ for which the conjugate spectral variances reach maximum and minimum values, V_{max}^+ and V_{min}^- respectively. A minimum uncertainty state obeys the equality $V_{max}^+ V_{min}^- = 1$. It is convenient to discuss our examples in terms of these quadratures. Suppose our input field is quantum noise limited but with a small classical signal imposed at an arbitrary quadrature angle. This is equivalent to a coherent state of a particular amplitude but unknown phase. For this input $V_{max}^+ = V_s + 1$ and $V_{min}^- = 1$, where V_s is the signal power. If $V_s = 2$ then spectral visibilities identical to the single photon counting visibilities will be observed. Alternatively the input state may be squeezed at some arbitrary angle such that $V_{max}^+ > 1 > V_{min}^-$. If $V_{max}^+ = 1/(2 - \sqrt{3})$ and $V_{min}^- = (2 - \sqrt{3})$ then again spectral visibilities will be identical to the single photon counting visibilities.

These results are significant as reliable teleportation of spectral components is technologically less challenging than single photon experiments and are thus likely to form a significant part of future quantum information research.

VI. CONCLUSION

We have examined an interferometric test of the efficacy of teleportation. Though more specific than other teleportation figures of merit, interferometric visibility is clearly of importance in applications of teleportation in quantum information processing. Unique characteristics of this arrangement are: (i) it doesn't require the tester to know the input state of the light, only the average power; (ii) the ability of the teleporter to reconstruct both the relative and global phase of the field is tested directly; and (iii) one can directly test the state reconstruction ability of the teleporter separately from or together with its efficiency.

The teleportation efficacy is characterized by the visibility between the two outputs of a Mach-Zehnder interferometer when the teleporter to be tested is placed in one of the arms. We have contrasted the results obtained with no entanglement and varying levels of squeezing entanglement using continuous variable teleportation. A clear classical limit (i.e. with no entanglement) to the visibility was demonstrated and its dependence on input average photon number investigated. For an average photon count of one per measurement interval the classical limit was $\mathcal{V} \leq \sqrt{1/5}$. Higher classical visibilities could be obtained with greater photon flux. The classical limit was lower with smaller photon flux. High visibilities (close to one) could only be obtained (for low photon flux) with high levels of entanglement and low levels of loss. These are the requirements for high efficiency teleportation. However decreased photon flux in the teleported arm (reduced efficiency) can be compensated by re-balancing the unteleported arm of the interferometer. In this way state reconstruction can be tested separately from efficiency. We find that, provided losses are small, ideal state reconstruction can be achieved for any level of entanglement squeezing. This is characterized by unit visibility in the balanced interferometer with finite levels of entanglement. Losses reduce visibilities but the general trends remain the same.

A generalization of the technique to continuous variable inputs was presented. With suitable interpretation it was found that the visibilities exhibited identical behavior to their discrete variable counterparts.

We believe that tests of the kind outlined in this paper will be essential if quantum teleportation is to be incorporated in reliable quantum information networks.

We wish to thank A.G.White and G.J.Milburn for helpful discussions. This work was supported by the Australian Research Council.

APPENDIX

Some readers may find it unusual that the classical channel a_c is described by an operator. This is a standard feature of the treatment of classical channels in the Heisenberg picture, *not* a consequence of our particular choice of an optical classical channel or our particular choice of teleporter model. The different treatments of classical channels between the Heisenberg and Schroedinger pictures are contrasted for quantum limited feedback in Ref. [20]. That a_c is truly a classical channel can be demonstrated easily via the no-cloning theorem [27] which states that a quantum system can not be duplicated without penalty. If the quantum nature of a_c is significant in the teleportation process then the no-cloning theorem would predict that duplication of a_c would lead to a significant degradation in the quality of the teleported state. An optimum continuous variable cloner can be constructed from the combination of a linear amplifier of gain 2 followed by a 50:50 beamsplitter. Applying this to a_c produces the two clones a'_c and a''_c given by

$$\begin{aligned} a'_c &= a_c + \frac{1}{\sqrt{2}}(v_{c1}^\dagger + v_{c2}) \\ a''_c &= a_c + \frac{1}{\sqrt{2}}(v_{c3}^\dagger - v_{c2}) \end{aligned} \quad (34)$$

where the v 's are vacuum modes. Suppose Bob uses a'_c for the reconstruction. He will produce the output

$$a_{out} = \lambda a_{in} + (\lambda\sqrt{H} - \sqrt{H-1})v_3^\dagger + (\sqrt{H} - \lambda\sqrt{H-1})v_4 + \sqrt{\varepsilon}\frac{1}{\sqrt{2}}(v_{c1}^\dagger + v_{c2}) \quad (35)$$

The final term is due to the cloning process. But in the classical channel limit we have $\varepsilon \rightarrow 0$ and hence this final term can be neglected and Eq.6 reduces to Eq.35. Arbitrarily good reconstruction of the input beam is still possible. A same result holds if Bob were to use the other clone, a''_c , for the reconstruction. Thus the cloning procedure does not change the quantum properties of the output and so a_c must be considered a classical channel.

REFERENCES

- [1] R. Landauer, Physics Today, 23 (May 1991).
- [2] C. H. Bennett and D. P. DiVincenzo, Nature, **404**, 247 (2000).
- [3] C. H. Bennett, G. Brassard, C. Crepeau, R. Jozsa, A. Peres and W. K. Wootters, Phys. Rev. Lett. , **70**, 1895 (1993).
- [4] D. Bouwmeester, J-W. Pan, K. Mattle, M. Eibl, H. Weinfurter and A. Zeilinger, Nature (London) **390**, 575 (1997).
- [5] D. Boschi, S. Branca, F. De. Martini, L. Hardy and S. Popescu, Phys. Rev. Lett. **80**, 1121 (1998).
- [6] Jian-Wei Pan, Dik Bouwmeester, Harald Weinfurter and Anton Zeilinger, Phys. Rev. Lett. **80**, 3891 (1998).
- [7] A. Furusawa, J. L. Sorensen, S. L. Braunstein, C. A. Fuchs, H. J. Kimble and E. S. Polzik, Science, **282**, 706 (1998).
- [8] D. Deutsch and P. Hayden, to appear in the Proceedings of the Royal Society A, LANL e-print quant-ph/9906007 (1999).
- [9] B. Schumacher, Phys. Rev. A **51**, 2738 (1995).
- [10] T. C. Ralph and P. K. Lam, Phys. Rev. Lett. **81**, 5668 (1998).
- [11] T. C. Ralph, to appear in Springer Lecture Notes; Walls memorial volume, LANL e-print quant-ph/0004093 (2000).
- [12] T. C. Ralph, P. K. Lam and R. E. S. Polkinghorne, J.Opt.B **1**, 483 (1999).
- [13] T. C. Ralph, Phys. Rev. A **61**, 044301 (2000).
- [14] R. E. S. Polkinghorne and T. C. Ralph, Phys. Rev. Lett. **83**, 2095 (1999).
- [15] T. C. Ralph, Opt Lett **24**, 348 (1999).
- [16] S. L. Braunstein and H. J. Kimble, Phys. Rev. Lett. , **80**, 869 (1998).
- [17] Z. Y. Ou, S. F. Pereira, H. J. Kimble, and K. C. Peng, Phys. Rev. Lett. **68**, 3663 (1992).
- [18] G. Yeoman and S. M. Barnett, J.Mod.Opt, **40**, 1497 (1993).
- [19] Y. Yamamoto, S. Machida and O. Nilsson, Phys. Rev. A **34**, 4025 (1986).
- [20] H. M. Wiseman, Phys. Rev. A **49**, 2133 (1994).
- [21] S. L. Braunstein and H. J. Kimble, Nature **394**, 840 (1998).
- [22] D. Bouwmeester, J-W. Pan, H. Weinfurter and A. Zeilinger, LANL e-print quant-ph/9910043 (1999).
- [23] A. Imamoglu and Y. Yamamoto, Phys. Rev. Lett. **72**, 210 (1994).
- [24] B. Lounis and W. E. Moerner, preprint (2000).
- [25] In principle the criteria proposed in [10] can be used for mixed states.
- [26] H. Barnum, C. M. Caves, C. A. Fuchs, R. Jozsa and B. Schumacher, Phys. Rev. Lett. **76**, 2818 (1996).
- [27] W.K.Wooters and W. H. Zurek, Nature (London) **299**, 802 (1982).

FIGURES

FIG. 1. Schematics of all optical teleporter. In (a) a classical teleporter is shown (i.e. with no entanglement). In (b) the inclusion of entanglement (EPR) is shown. In (c) the separate teleportation of the two polarisation modes is represented. TV and TH are the teleporters for the vertical and horizontal polarisation components respectively. PBS stands for polarising beam-splitter.

FIG. 2. Schematic of the linear amplifier used in the teleporters. The PA's stand for parametric amplifiers which are pumped in phase (E) and out of phase ($-E$) with the field.

FIG. 3. Schematics of interferometric test arrangements

FIG. 4. Schematics of different input state-measurement techniques.

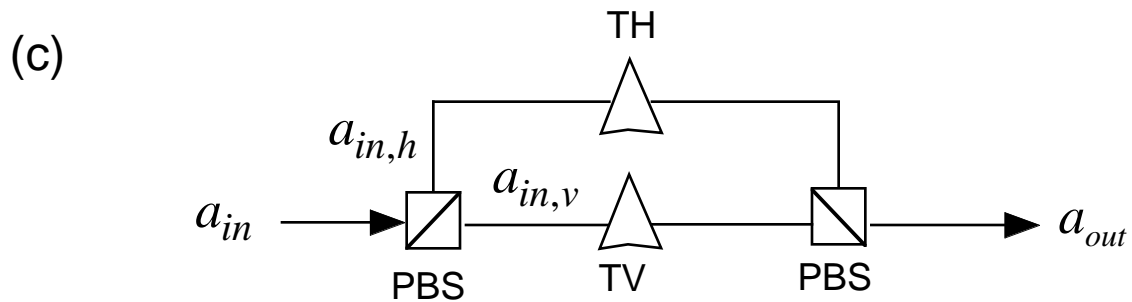
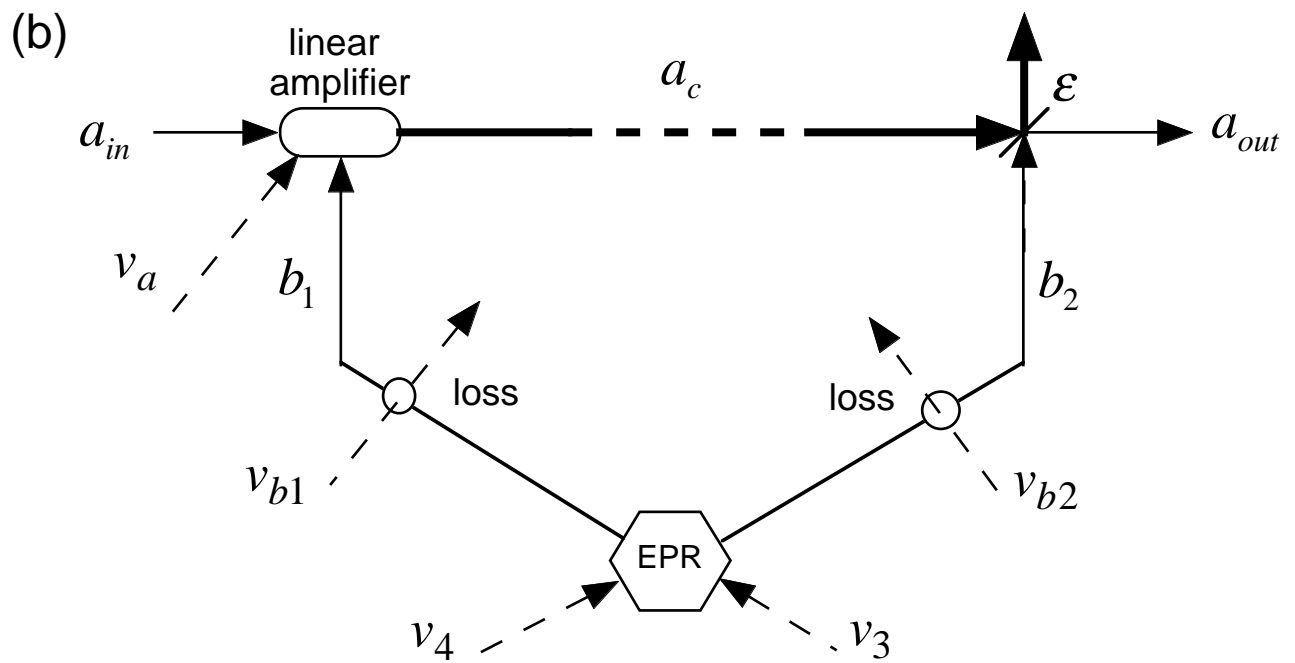
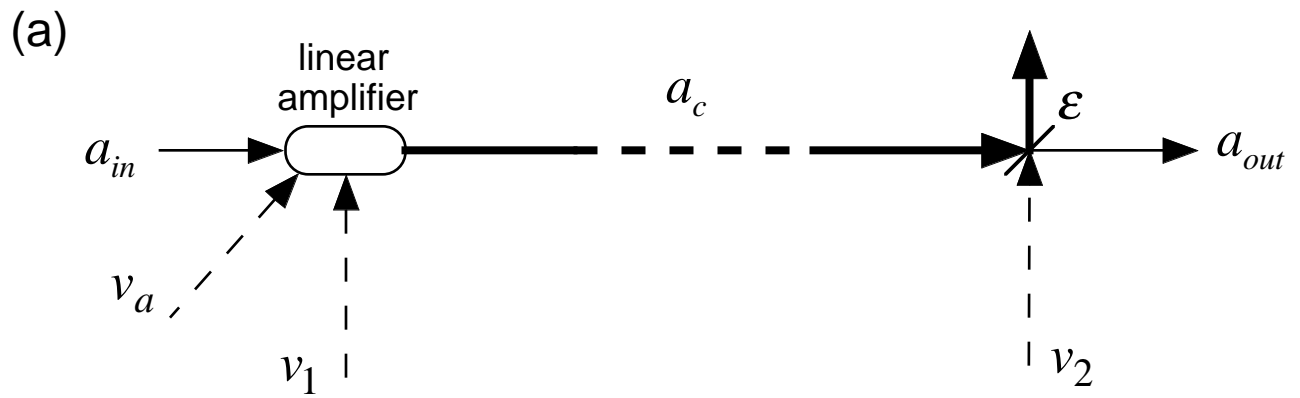
FIG. 5. Visibility versus gain for the set-up shown in Fig.3(a) and various levels of entanglement (0%, 50% and 90%).

FIG. 6. Visibility versus gain with “attenuation balancing” (set-up shown in Fig.3(b)) for various levels of entanglement (0%, 50% and 90%).

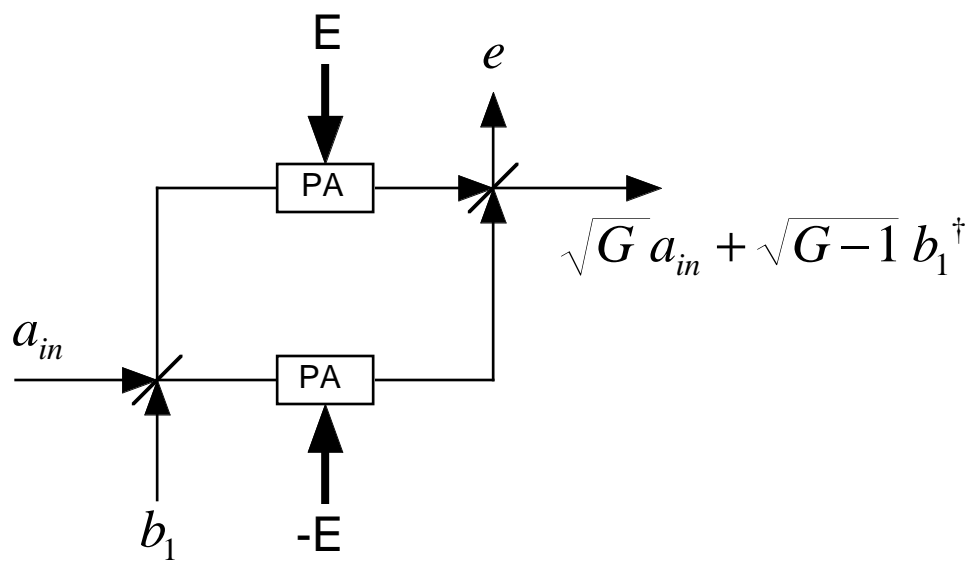
FIG. 7. The effect of loss on the visibility. In (a) the maximum visibility is plotted versus the transmission efficiency of the entangled beams for various levels of entanglement (0%, 50% and 90%). In (b) balancing of the interferometer is allowed (plot is for 50% entanglement)

FIG. 8. Gain for maximum visibility (λ_{max}^2) and maximum visibility thus achieved (V_{max}) versus level of entanglement for various average input photon numbers ($\bar{n} = 0.25, 1.0, 4.0$).

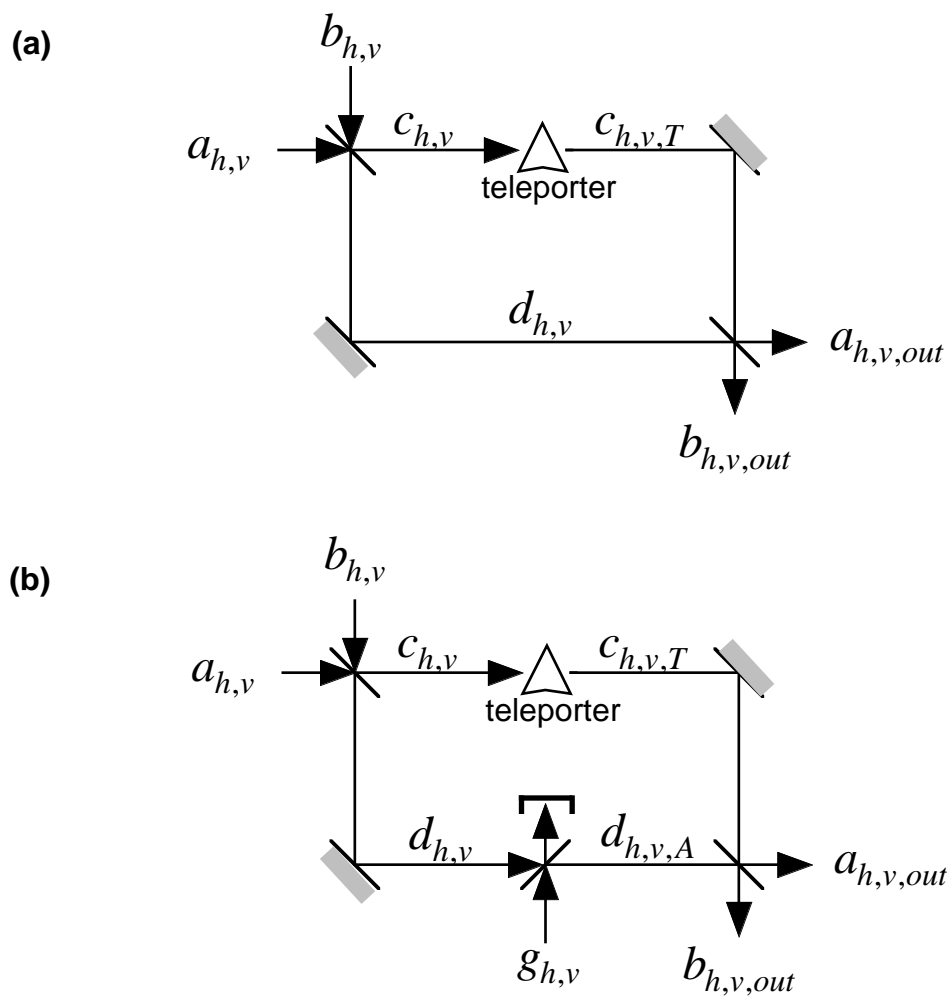
“Interferometric tests....” Ralph, Figure 1



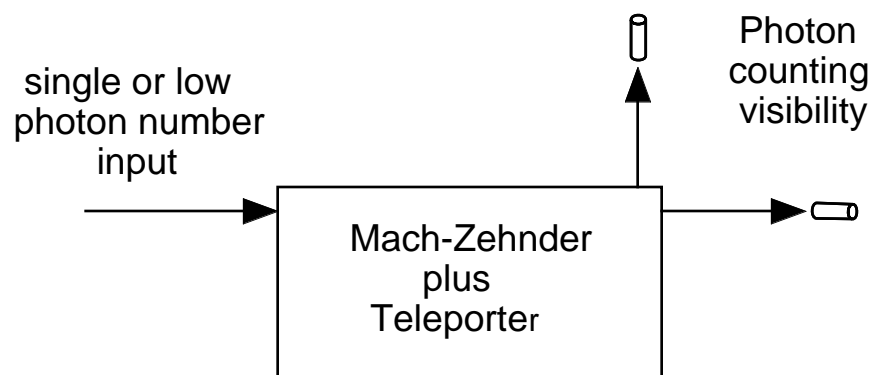
"Interferometric Tests..." Ralph, Figure 2



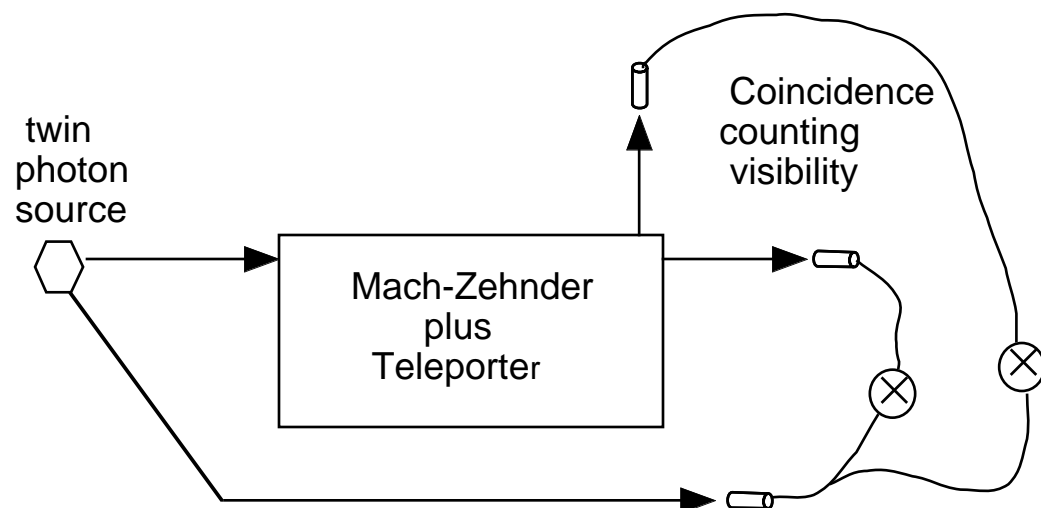
"Interferometric Tests...." Ralph, Figure 3



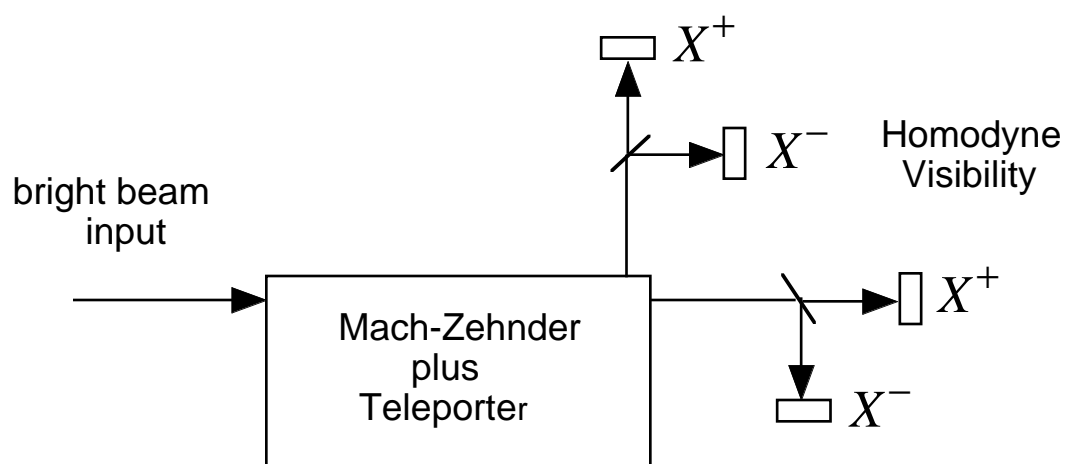
(a)



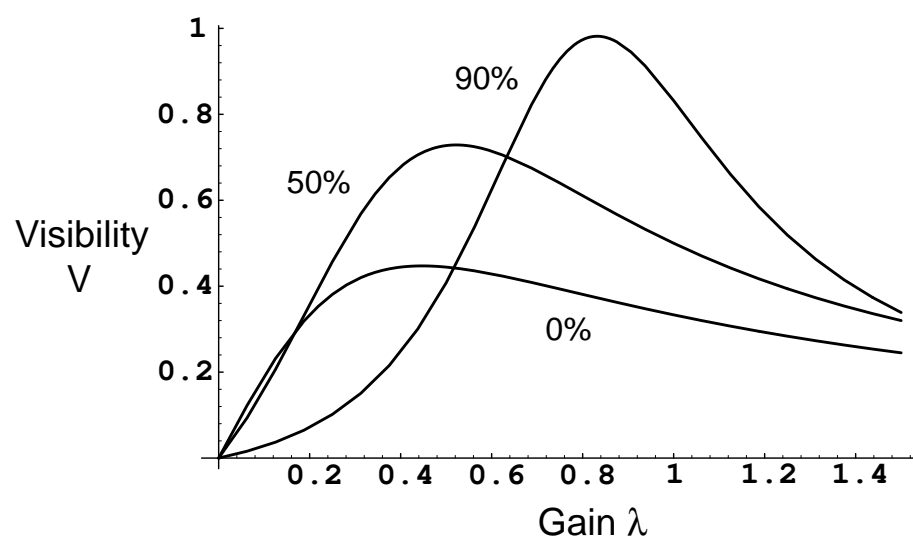
(b)



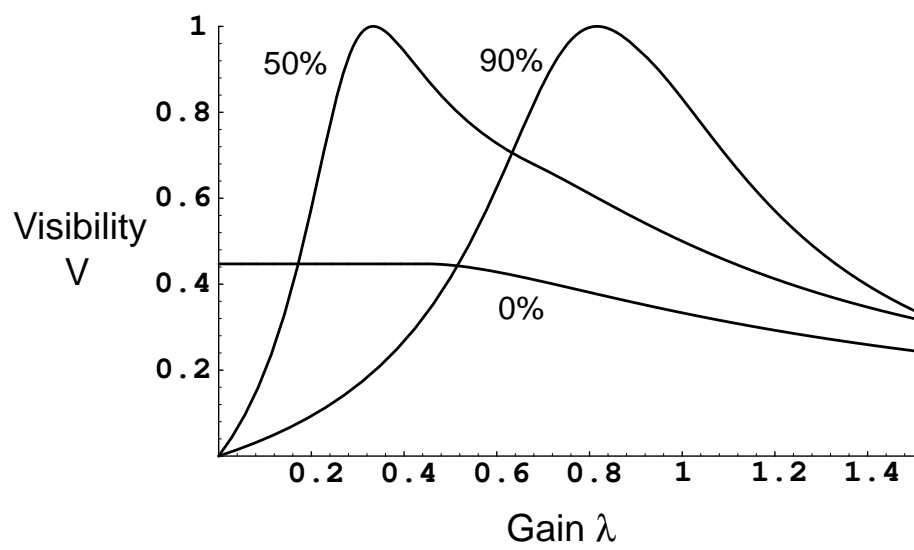
(c)



"Interferometric Tests...." Ralph, Figure 5

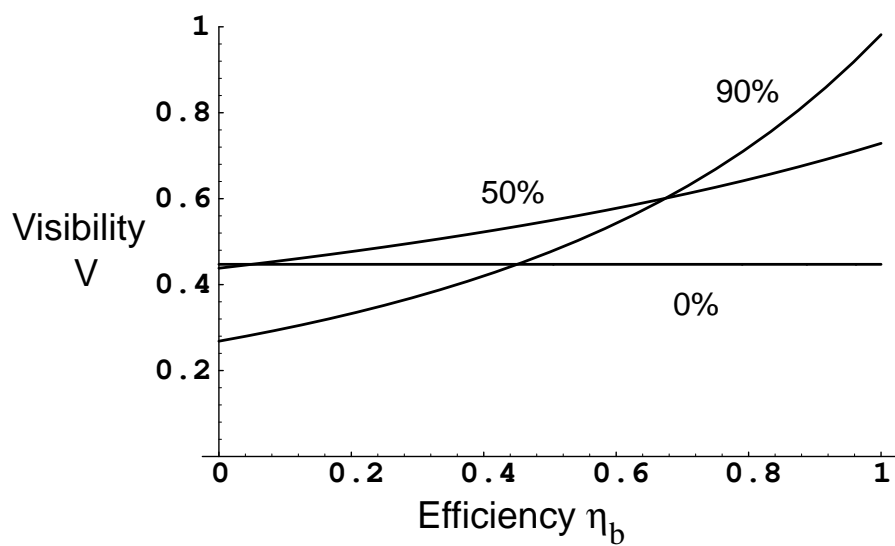


"Inteferometric Tests..." Ralph, Figure 6

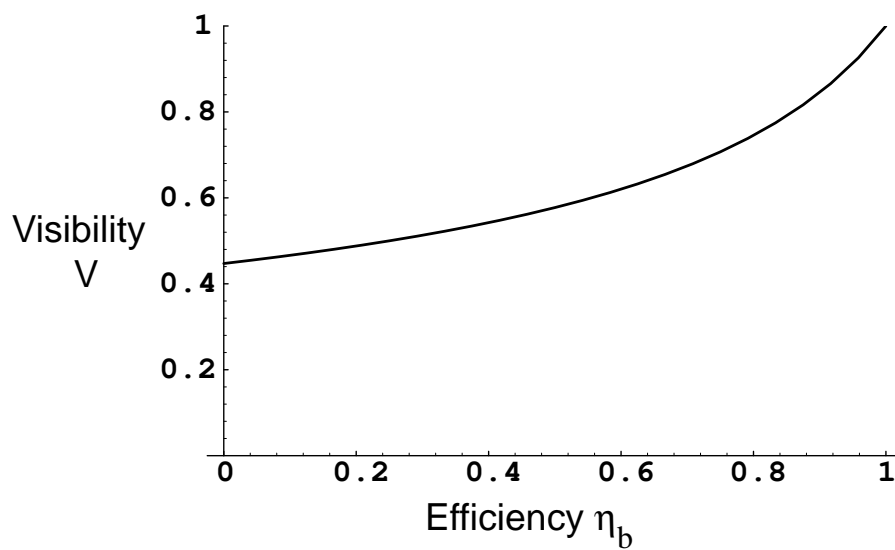


"InterferometricTests..." Ralph, Figure7

(a)



(b)



"Interferometric Tests..." Ralph, Fig.8

